Am J Transl Res 2018;10(11):3857-3875
www.ajtr.org /ISSN:1943-8141/AJTR0074499

Original Article

SQYZ granules, a traditional Chinese herbal, attenuate cognitive deficits in AD transgenic mice by modulating on multiple pathogenesis processes

Haiting An[1,2,3], Dongfeng Wei[4], Yanjing Qian[1,2,3], Ning Li[1,2,3], Xiaomin Wang[1,2,3]

[1]Department of Neurobiology, Capital Medical University, Beijing 100069, China; [2]Key Laboratory for The Neurodegenerative Disorders of the Chinese Ministry of Education, Beijing 100069, China; [3]Beijing Institute for Brain Disorders, Beijing 100069, China; [4]Institute of Basic Research in Clinical Medicine, China Academy of Chinese Medical Sciences, Beijing 100700, China

Received February 12, 2018; Accepted May 14, 2018; Epub November 15, 2018; Published November 30, 2018

Abstract: The pathogenesis of Alzheimer's disease (AD) involves multiple contributing factors, including amyloid β (Aβ) peptide aggregation, inflammation, oxidative stress, and others. Effective therapeutic drugs for treating AD are urgently needed. SQYZ granules (SQYZ), a Chinese herbal preparation, are mainly composed of the ginsenoside Rg1, astragaloside A and baicalin, and have been widely used to treat dementias for decades in China. In this study, we found the therapeutic effects of SQYZ on the cognitive impairments in an AD mouse model, the β-amyloid precursor protein (APP) and presenilin-1 (PS1) double-transgenic mouse, which co-expresses five familial AD mutations (5XFAD); next, we further explored the underlying mechanism and observed that after SQYZ treatment, the Aβ burden and inflammatory reactions in the brain were significantly attenuated. Through a proteomic approach, we found that SQYZ regulated the expression of 27 proteins, mainly those related to neuroinflammation, stress responses and energy metabolism. These results suggested that SQYZ has the ability to improve the cognitive impairment and ameliorate the neural pathological changes in AD, and the therapeutic mechanism may be related to the modulation of multiple processes related to AD pathogenesis, especially anti-neuroinflammation, promotion of stress recovery and improvement of energy metabolism.

Keywords: Alzheimer's disease, SQYZ granules, 5XFAD mice, traditional Chinese medicine, proteomics

Introduction

The prevalence of dementia continues to increase across all regions of the world, due to the ageing population. Alzheimer's disease (AD), as the main cause of dementia, is one of the great health-care challenges of the 21st century [1]. AD mainly manifests as progressive and irreversible cognitive impairments, including memory loss and deficits in learning and working, which are underlain by severe neurodegeneration in the brain. During the past 30 years, remarkable advances have been achieved in AD research, especially in regard to AD pathogenesis. A substantial amount of evidence has shown that the accumulation of abnormally folded Aβ proteins in amyloid senile plaques (SP) and tau proteins in neurofibrillary tangles (NFTs) are causally related to the neurodegenerative processes in the brains of AD patients [2]. In addition, on a deeper level, the complexity and multicausality of AD, i.e., it is caused by a number of genetic and environmental factors, have been recognized [3, 4]. It is well accepted that multiple factors, including apoptosis, oxidative stress, mitochondrial dysfunction, inflammatory responses, and disturbances in energy metabolism homeostasis, are involved in the progression of AD [4, 5].

However, the therapy for AD is not yet satisfactory. Currently, only four therapeutic agents (donepezil, rivastigmine, galantamine and memantine) for AD have been approved by the US Food and Drug Administration (FDA) [6]. They only have modest effects, which are limited to merely relieving the symptoms, rather than to prevent or reverse the pathological core of AD

[7]. The reason for this poor situation may lie in the complexity of AD pathogenesis, which renders drugs aimed at a single process less efficient. Thus, treatments that intervene in multiple targets in AD may be a hopeful resolution [5].

Traditional Chinese medicine (TCM) has a long history in China. It usually uses combinations of herbs or herbal ingredients to treat diseases, with the components targeting different disease processes. SQYZ granules (SQYZ), a TCM herb, consists mainly of three natural components, including the ginsenoside Rg1, astragaloside A and baicalin. These three components have a wide range of activities, including anti-inflammation, antioxidation, promotion of neurogenesis, neuroprotection, etc., which are all key points in the therapy of AD [8, 9]. SQYZ has been commonly used in the clinical treatment of dementia in China, exerting a potent role in curing AD. However, the therapeutic mechanism of SQYZ in AD has not been well elucidated. In the present study, we used a transgenic mouse model, 5XFAD, to evaluate the therapeutic effects of SQYZ, and further to elucidate the underlying mechanisms of this preparation. This study may be significant for the therapy and prevention of AD.

Materials and methods

Animals

APP/PS1 double transgenic mice, known as 5XFAD, co-express the human APP and PS1 transgenes (number 006554, Jackson Laboratory) and contain five familial AD mutations (APP*Sw*Fl*Lon, PSEN1*M146L*L286V) under the transcriptional control of the neuron-specific mouse Thy1 promoter. The transgenic mice were originally obtained from Jackson Laboratory and backcrossed to C57BL/6J at least 5 generations to achieve C57BL genetic identity. After that, the transgenic mice were maintained by crossing heterozygous transgenic mice with C57BL/6J wild-type breeders. Genotyping was performed using PCR analysis of tail DNA. Animals were housed in cages in a controlled environment (22-25°C, 50% humidity and a 12-hour light/dark cycle) with free access to standard laboratory chow and distilled water. All efforts were made to minimize both animal suffering and the number of animals used. All procedures performed in this study were in accordance with the Chinese regulations involving animal protection and were approved by the animal ethics committee of the China Capital Medical University.

Drug treatments

SQYZ was supplied by China Academy of Chinese Medical Sciences (lot number: 2014-0508). Huperzine-A (HupA), as a positive control drug, was purchased from Beijing Century Aoke Biotechnology Co. Ltd. (lot number: MUST-13102808). These drugs were stored at 4°C. Mice were randomly divided into five groups, including normal saline-treated WT (WT+NS) and transgenic (Tg+NS) mouse groups; SQYZ-treated WT (WT+SQYZ) and transgenic (Tg+SQYZ) mouse groups; and a HupA-treated transgenic mouse group (Tg+HupA). Four-month-old female transgenic mice in the medicine-treated groups were administrated orally of 5.55 g/kg SQYZ or 0.1 mg/kg HupA, once per day for 60 days, whereas the other two groups were treated with same volume of normal saline as controls.

Behavioral tests

Morris water maze test: The Morris water maze test was performed to assess the learning and memory abilities of the mice [10]. The pool was arbitrarily divided into four quadrants, namely, the training, adjacent left, adjacent right and opposite quadrants. On the first day, the mice were initially introduced to the visible platform to habituate them to the experimental environment. Then, the platform was moved to another quadrant and hidden beneath the surface of the water. Mice then underwent three trials per day for five consecutive days to measure their ability to navigate to the hidden platform. Twenty-four hours after the last training day, all mice were given a probe test for 30 seconds, during which the platform was removed from the pool, and the time taken to cross to the quadrant originally containing the platform was assessed.

Passive avoidance test: The passive avoidance test is a fear-motivated test that is used to study memories in an associative manner [11]. It requires the animal to behave in a manner opposite to its innate dark preference. The test was performed using a shuttle-box apparatus, which consists of two compartments separated

by a door. One compartment was lit with a bright, cold house light and served as the safe compartment, while the other was made with a dark, opaque wall and served as the unsafe side. On the first day, the mice were put into the light side for 5 minutes of habituation. During training, the mice received an electric shock (0.03 mA, 2 s duration) delivered through the grid floor when they stepped into the dark sides. On the second day, the mice were placed back into the same testing box, but no shock was applied, and the initial latency and times to enter the dark side were recorded.

Nest construction test: The nest construction test was performed according to the previous description [12]. In brief, after mice were single housed for 16 hours in clean plastic cages, eight pieces of paper towels (4 cm × 4 cm) were introduced inside home cages for nesting. Next day (16 hours later), cages were inspected for nesting evaluation. The score was assessed on a rating scale of 1-4 with 1 ≥ 50% of paper towels remaining intact and spreading around the cage, 2 ≤ 50% of paper towels remaining intact but no nestle in a corner of the cage, 3 ≥ 90% of paper towels torn and grouped into a corner of the cage and 4 = a perfect nest constructed by < 1 cm pieces and grouped into a corner of the cage.

Immunofluorescence

After the behavioral tests were completed, the mice were anaesthetized using 10% chloral hydrate (7.5 ml/kg of body weight, intraperitoneal) and then transcardially perfused with 0.9% sodium solution and decapitated. One brain hemisphere from each mouse was snap-frozen for biochemical assays. The other hemibrain of each mouse was fixed in 4% paraformaldehyde in PBS and cryoprotected in 30% sucrose solution in 0.01 M PBS. Brains were sectioned along the coronal plane using a freezing microtome at 30 μm and allowed to air dry on glass slides. The primary antibodies were rabbit polyclonal anti-Iba1 (1:200; 019-19741, Wako) and rabbit polyclonal anti-GFAP (1:500; MAB360, Millipore). Goat anti-rabbit IgG Alexa Fluor 488 (1:500, A-11034, Invitrogen) and goat anti-rabbit IgG Alexa Fluor 594 (1:500, A-11012, Invitrogen) were used as secondary antibodies. Images were captured under a microscope equipped with a digital camera (Olympus). The fluorescence intensity of GFAP and Iba1 were quantified using the Image-Pro Plus 6.0 software, according to our previous description [13]. The value was normalized to the total cortex area in the 100× image. For each mouse, the averages were calculated across images such that each animal only contributed a single value.

Western blot and ELISA

For western blotting, frozen cortex tissues were homogenized in RIPA buffer (50 mM Tris, pH 7.4, 150 mM NaCl, 1% Triton X-100, 1% sodium deoxycholate, 0.1% SDS) containing protease inhibitor cocktail (1:100, Sigma) and were then centrifuged at 12,000 g for 15 minutes at 4°C. The supernatants were collected, and total protein levels were quantified via the BCA protein assay kit (Pierce). Equal amounts of protein (30 μg) were separated on 10% SDS-PAGE gels and were transferred to nitrocellulose membranes (Millipore). After blocking, the membranes were simultaneously labelled with antibodies, rabbit polyclonal anti-MAPK3 (1:1000; 137F5, Cell Signaling Technology), mouse monoclonal anti-dynamin-1 (1:2000; 2441931, Millipore) and mouse monoclonal anti-α-tubulin (1:5000; T8203, Sigma). Next, the primary antibody-labelled membranes were treated with secondary antibodies, goat anti-mouse IgG, HRP conjugated (1:10000; CW0102A, CWBIO) and goat anti-rabbit IgG, HRP conjugated (1:10000; CW0103A, CWBIO). The bands were then visualized using the FluorChem E imaging system (protein simple) and analyzed by ImageJ software.

Human Aβ42 levels were assessed using a sandwich ELISA. Frozen brain tissues treated with RIPA lysis buffer were centrifuged, and then the soluble supernatant fractions were collected. The insoluble materials were dissolved with lysis buffer (8% SDS, 8 M urea and 5 mM EDTA). The soluble and insoluble Aβ42 were quantified using human Aβ42 ELISA kits (KHB3441, Invitrogen), following the manufacturer's instructions. The absorbance was read at 450 nm using a 96-well plate reader, and Aβ levels were calculated from a standard curve and normalized to the total protein levels, determined by the BCA protein assay kit (Pierce).

Two-dimensional electrophoresis and gel image analysis

Two-dimensional electrophoresis (2-DE) was performed according to a previously reported

protocol [14]. The protein pellets from the cortices of two groups of mice (Tg+NS and Tg+SQYZ) were dissolved in sample buffer (7 M urea, 2 M thiourea, 4% (w/v) CHAPS, 65 mM DTT, 0.5% (v/v) Bio-lyte ampholytes). The protein was quantified by the Bradford assay. After the process of 2-DE [14], the SDS/PAGE gels were stained with Coomassie Brilliant Blue solution containing 2% (v/v) phosphoric acid, 10% (w/v) ammonium sulfate, 20% (v/v) methanol, and 0.1% (w/v) G-250 overnight [15]. Three replicates for each group were acquired for the gel analyses. The obtained 2-DE gels were scanned using a GS-calibrated densitometer (Bio-Rad) and analysed with the software PDQuest 8.0.1 (Bio-Rad). Quantitative analysis of the protein spots was achieved by calculating the average and normalizing the spot volumes among the gel images of the protein profiles obtained from the Tg+NS and Tg+SQYZ groups. The total spot volume normalization algorithm was used to calculate each protein spot volume as the sum of the intensities of the pixels within the spot's boundary minus the background level within that same boundary normalized to the total spot volumes in the gel [16]. The protein spots that showed a statistically significant change in volume ($P < 0.05$, Student's t-test) of at least 1.5-fold were selected and subjected to further evaluation with MALDI-TOF MS/MS [17].

Protein identification by MALDI-TOF-MS/MS and database searching

The differentially expressed protein spots were excised from Coomassie-stained 2-DE gels, washed with Milli-Q water three times, and then destained with 25 mM NH_4HCO_3/50% ACN. After being washed with 100% ACN for 5 min, the destained gel pieces were dried and then rehydrated with 0.02 g/l trypsin (Promega Corp.) solution for 30 min. The excess liquid was removed, and the pieces of the gel were immersed in 25 mM NH_4HCO_3 containing 10% acetonitrile overnight at 37°C. The digests were desalted with ZiptipTM (C-18, Millipore), according to the manufacturer's instructions and were subjected to an analysis using MALDI-TOF MS. Single MS and tandem mass spectrometer (MS/MS) experiments were performed with a hybrid QSTAR Pulsar I quadrupole time-of-flight mass spectrometer (Applied Biosystems/MDS Sciex, Toronto, Canada) equipped with a nano-ESI ion source. The proteins were identified in both the Tg+NS and Tg+SQYZ groups, and two or more sequences were analysed for one spot in our study. For PMF identification, the peptide mass maps were searched against the NCBI protein sequence database using an in-house MASCOT (version 2.1, Matrix Science, UK) search engine. For the peptide mass fingerprints (PMFs), the search conditions included the following: type of search set as MS/MS Ion Search, enzyme set as trypsin, and alkylation of cysteine by carbamidomethylation as a fixed modification. Standard search parameters were set to allow the mass tolerance of 0.1 Da and 2 missed tryptic cleavages.

Statistical analysis

All values were shown as the mean ± standard error of mean (SEM). Statistical analysis was performed using Prism5.0 (GraphPad Software). Statistical analyses of the behavioral tests, ELISA and immunofluorescence data were performed using analysis of one-way ANOVA followed by Tukey's post hoc test. The results of proteomic were compared between Tg+NS and Tg+SQYZ groups with Student's t-test. *P* values < 0.05 were considered statistically significant.

Results

SQYZ prevented cognitive behavioral impairments of AD transgenic mice

According to our previous work, 4-month-old female AD transgenic mice, i.e., at the early stage of AD [10, 18], were selected to assess the effects of SQYZ treatment. After 60 days of treatment with SQYZ, behavioral tests were performed on the mice, including the Morris water maze, passive avoidance and nest construction tests. The Morris water maze test was used to evaluate the mice for spatial learning and memory deficits. During the acquisition test, the Tg+NS group exhibited significantly complicated escape pathways and prolonged escape latencies after 3 days of training compared to the WT+NS group ($P < 0.05$), while the SQYZ and HupA treatments prevented the increase in escape latency in the 5XFAD mice (**Figure 1A**, **1B**). In the probe test, the percentage of time spent in the target quadrant (**Figure 1C**) significantly decreased in the Tg+NS group compared to the WT+NS group ($P < 0.01$), while the SQYZ and HupA treatments prevented this

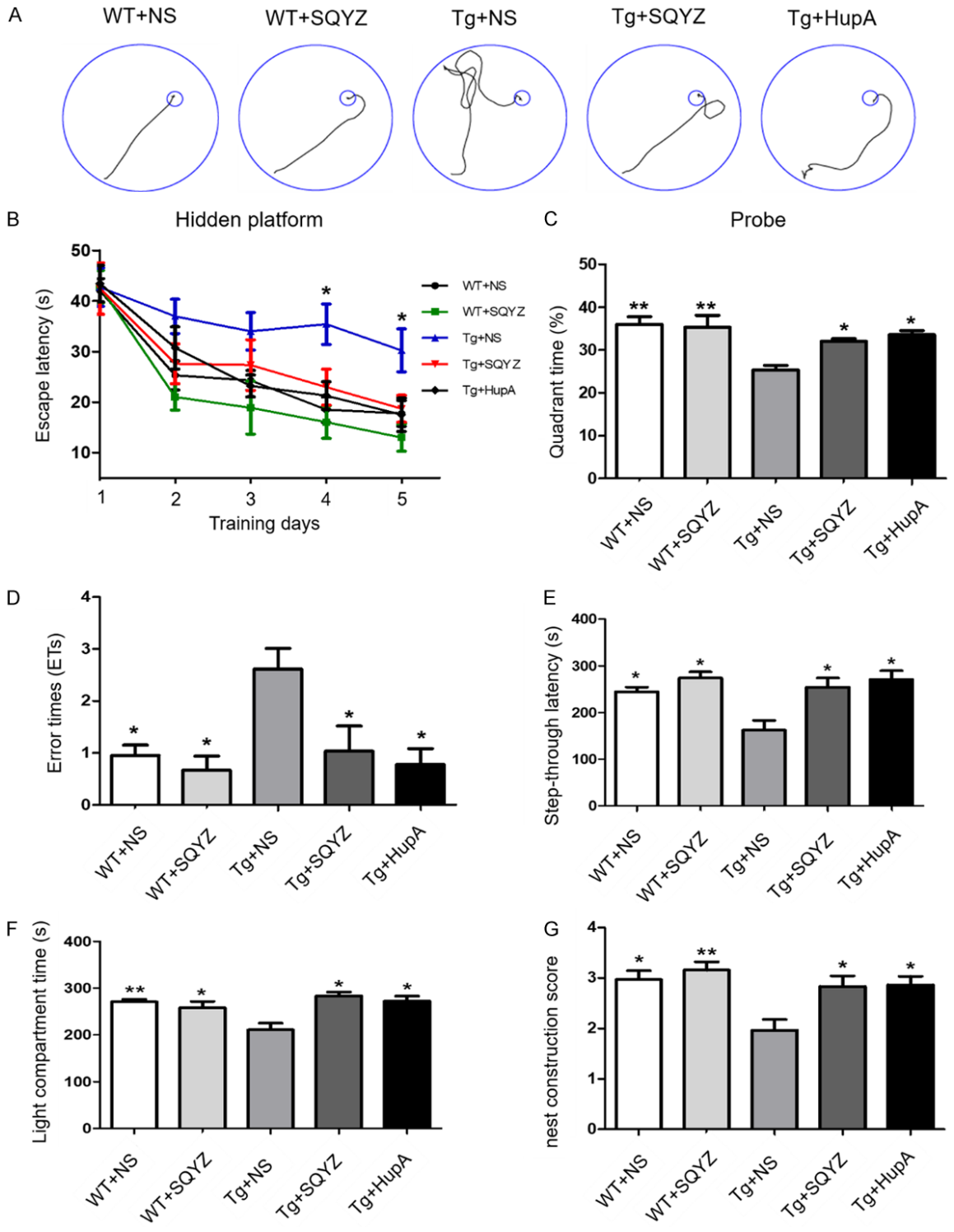

Figure 1. SQYZ treatment improved AD behavioral performances of 5XFAD mice. In the Morris water maze, during the hidden platform task, the escape strategies on the fifth day of training (A) of the WT+NS, WT+SQYZ, Tg+NS, Tg+SQYZ, and Tg+HupA groups were detected by using a camera. (B) The escape latency required for the mice to find the hidden platform on each training day was recorded. During the probe trial, one day after finishing the acquisition task, the time required to cross over to the target quadrant (C) was originally used to determine the memory retention of the mice. In the passive avoidance test, one day after fear training, the error times of mice entering the dark field (D), the step-through latency of mice from light side to dark side (E) and the time spent in light compartment (F) were recorded to test the fear memory abilities of the mice. During the nest construction test, the nesting scores of mice (G) were evaluated to reflect the abilities of daily living. All values were represented as the mean ± SEM, n = 13-15/group. *, $P < 0.05$, **, $P < 0.01$ vs. Tg+NS, one-way ANOVA with Tukey's post hoc test.

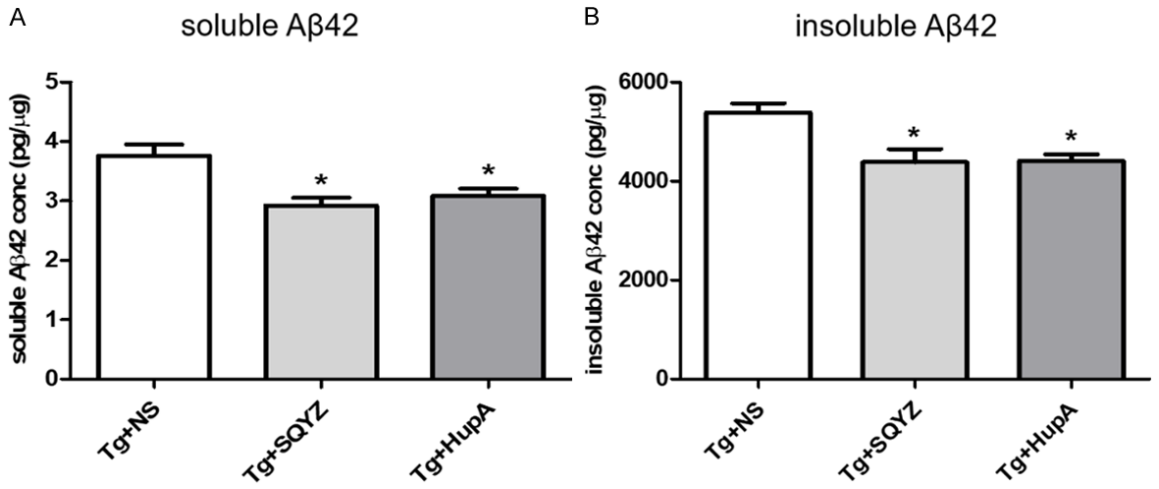

Figure 2. SQYZ reduced the levels of Aβ42 in the cortex of the AD transgenic mice. The soluble (A) and the insoluble Aβ42 levels (B) in the cortex of Tg+NS, Tg+SQYZ, and Tg+HupA mouse groups were tested by the ELISA assay. The Aβ concentration was normalized to total protein level in cortex. All values were represented as the mean ± SEM, n = 6/group. *, $P < 0.05$ vs. Tg+NS, one-way ANOVA with Tukey's post hoc test.

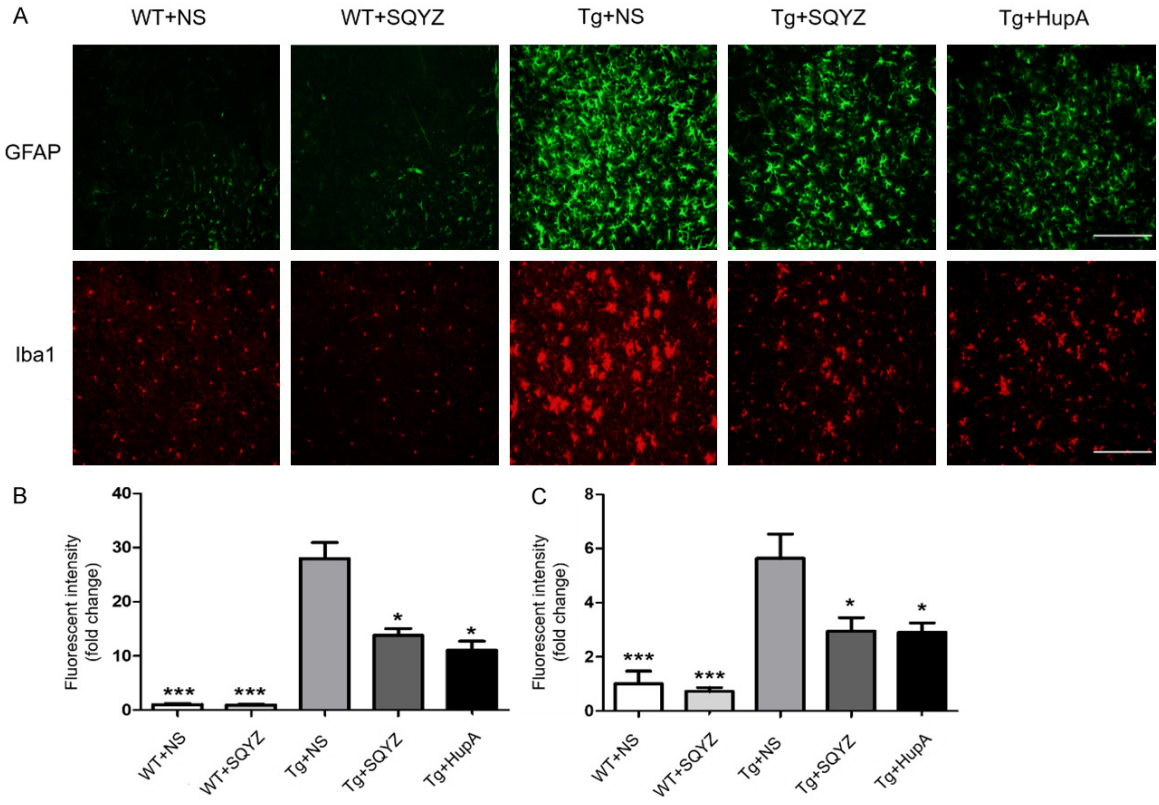

Figure 3. SQYZ treatment inhibited the activation of astrocyte and microglia in the cortex of 5XFAD mice. (A) Astrocytes and microglia in the cortex of the five groups were detected by immunofluorescence with antibodies against GFAP or Iba1. The fluorescence intensity of GFAP-positive (B) and Iba1-positive cells (C) of the five groups in the cortex were quantified using Image-Pro Plus 6.0 software. All values were represented as the mean ± SEM, n = 6/group. *, $P < 0.05$, ***, $P < 0.001$ vs. Tg+NS, one-way ANOVA with Tukey's post hoc test. Scale bar = 200 μm.

decline ($P < 0.05$). Thus, SQYZ treatment could improve the spatial memory acquisition and retrieval of 5XFAD mice. In passive avoidance test, the 5XFAD mice showed significantly

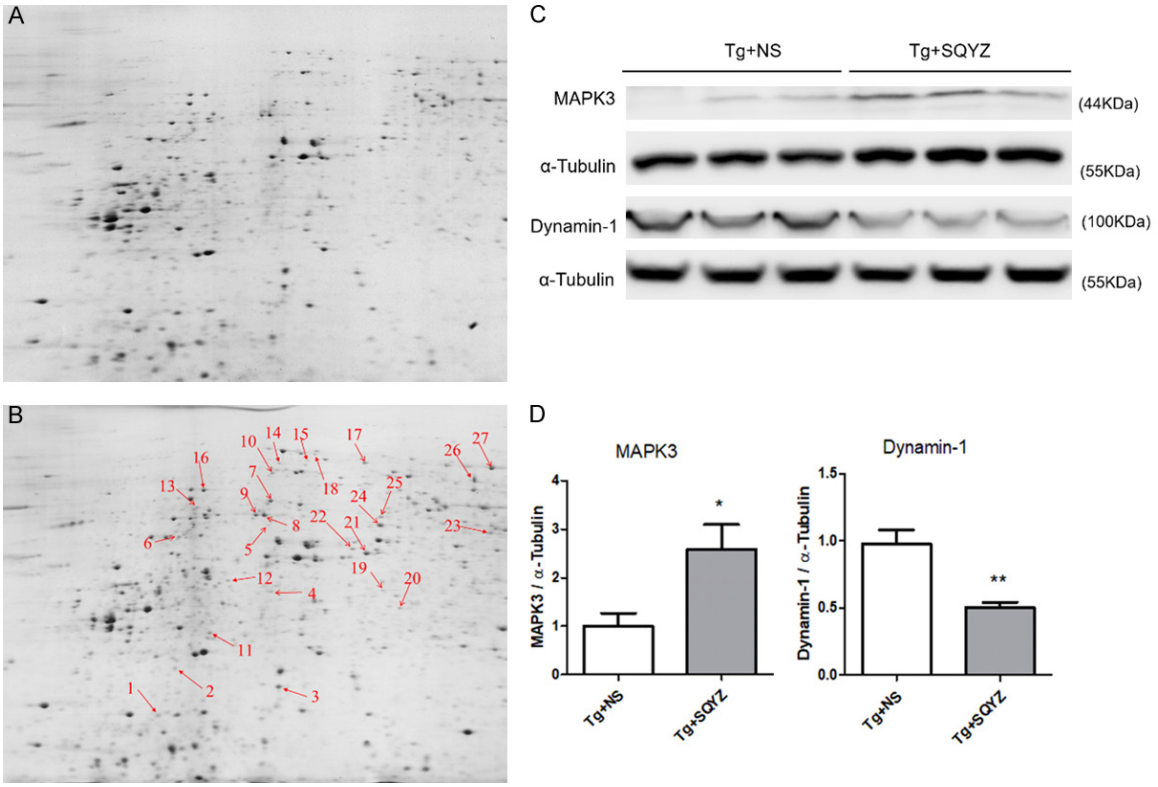

Figure 4. The differentially expressed proteins in SQYZ treated 5XFAD mouse were revealed by proteomic analysis. The protein spots that exhibited a statistically significant change ($P < 0.05$ by Student's t-test) of at least a 1.5-fold increase or decrease intensity between the Tg+NS group (A) and the Tg+SQYZ group (B), were selected and labelled with red arrows in 2-DE gel. These proteins were subjected to further evaluation by MALDI-TOF MS/MS analysis and database searching. The expression levels of dynamin-1 and mitogen-activated protein kinase 3 (MAPK3) were determined by western blot analysis of the cortices of the Tg+SQYZ and Tg+NS groups (C). The full gel pictures for immunoblots were shown in Supplementary Figure 1. The graphs (D) showed the relative expression quantifications of each protein (normalized to α-tubulin). Data were presented as the mean ± SEM, and statistical significance was determined by Student's t-test, n = 3/group, *, $P < 0.05$, **, $P < 0.01$ compared with the Tg+NS group.

increased error times ($P < 0.05$), reduced step-through latencies ($P < 0.05$) and a decreased amount of time spent in the light compartment ($P < 0.01$) compared to the WT mice (**Figure 1D-F**). The SQYZ treatment returned these indices to the normal level ($P < 0.05$), and HupA did in a similar manner ($P < 0.05$), suggesting that SQYZ treatment also improved the fear memory ability of the 5XFAD mice. To observe the effect of SQYZ treatment on activities of daily living, mice were subjected to the nest construction test (**Figure 1G**). Compared with the WT mice, the 5XFAD mice exhibited decreased nesting scores ($P < 0.05$). Meanwhile, increased scores of the 5XFAD mice were observed after the SQYZ and HupA treatments ($P < 0.05$). There was no significant difference between the score of the Tg+SQYZ group and that of the Tg+HupA group. This result implied that the SQYZ treatment improved the self-care ability of the 5XFAD mice, and importantly, the effect of SQYZ was comparable to that of HupA. It was noteworthy that SQYZ had no effect on the WT mice when compared to the WT mice treated with saline. In general, SQYZ improved cognitive behavioral performances of 5XFAD mice.

Treatment with SQYZ attenuated the Aβ burden in AD transgenic brains

To detect whether SQYZ change Aβ load in the brains of the AD transgenic mice, we used a sandwich ELISA to measure the levels of soluble and insoluble Aβ42 in the cortex of the transgenic mice that had been treated with SQYZ, HupA or saline. The results revealed that the concentrations of both soluble (**Figure 2A**) and insoluble Aβ42 (**Figure 2B**) in cortex of the 5XFAD mice were significantly reduced in response to the SQYZ or HupA treatment ($P <$

Table 1. The identification results of differentially expressed protein spots between the Tg+SQYZ and Tg+NS groups using LC-MS/MS

Number	Accession NO.	Target protein	Symbol	Exp. Mr (KDa)	Exp. pI	Protein Score	Fold difference	*P* value
1	P39053	Dynamin-1	Dnm1	97.8	7.61	253	0.11	0.001
2	Q64288	Olfactory marker protein	Omp	18.8	5.00	594	2.08	0.014
3	Q9CR95	Adaptin ear-binding coat-associated protein 1	Necap1	29.6	5.97	55	0.22	0.037
4	Q6PNC0	DmX-like protein 1	Dmxl1	336.0	5.97	33	2.09	0.022
5	Q9JI13	Something about silencing protein 10	Utp3	53.3	5.44	32	2.44	0.008
6	P50396	Guanosine diphosphate (GDP) dissociation inhibitor 1	Gdi1	51.0	4.96	31	0.5	0.045
7	P70270	DNA repair and recombination protein RAD54-like	Rad54l	84.6	9.58	31	2.32	0.004
8	Q9JJW5	Myozenin-2	Myoz2	29.7	8.53	34	3.73	0.0001
9	P60710	Actin, cytoplasmic 1	Actb	42.1	5.29	554	2.24	0.001
10	P63038	60 kDa heat shock protein, mitochondrial	Hspd1	60.9	5.91	70	2.03	0.001
11	Q9CPU0	Lactoylglutathione lyase	Glo1	20.8	5.24	201	4.64	0.003
12	Q9ERD7	Tubulin beta-3 chain	Tubb3	50.8	4.82	587	2.09	0.02
13	P56480	ATP synthase subunit beta, mitochondrial	Atp5b	56.3	5.19	44	3.13	0.0001
14	P63017	Heat shock cognate 71 kDa protein	Hspa8	71.1	5.37	335	4.32	0.0001
15	P38647	Stress-70 protein, mitochondrial	Hspa9	73.7	5.81	246	3.04	0.004
16	P46660	Alpha-internexin	Ina	55.5	5.35	62	2.00	0.0206
17	Q9JKK7	Tropomodulin-2	Tmod2	39.5	5.28	107	0.03	0.0001
18	Q05816	Fatty acid binding protein 5, epidermal	Fabp5	15.1	5.81	478	12.11	0.008
19	P16125	L-lactate dehydrogenase B chain	Ldhb	36.8	5.70	160	5.14	0.001
20	Q9CWS0	N(G), N(G)-dimethylarginine dimethylaminohydrolase	Ddah1	31.8	5.64	422	2.73	0.002
21	P42669	Transcriptional activator protein Pur-alpha	Pura	34.8	6.07	376	2.03	0.003
22	Q63844	Mitogen-activated protein kinase 3	Mapk3	43.0	7.57	340	2.66	0.015
23	Q7TMM9	Tubulin beta-2A	Tubb2a	49.9	4.78	36	2.14	0.002
24	P17182	Alpha-enolase	Eno1	47.1	4.74	318	3.66	0.001
25	O08553	Dihydropyrimidinase-related protein 2	Dpysl2	62.2	5.95	675	1.98	0.013
26	Q8BMF4	Dihydrolipoyllysine-residue acetyltransferase component of pyruvate dehydrogenase complex, mitochondrial	Dlat	67.9	8.81	357	4.20	0.005
27	Q3UGR5	Haloacid dehalogenase-like hydrolase domain-containing protein 2	Hdhd2	28.9	5.70	478	12.11	0.008

Note: The table showed the identification results of 27 differentially expressed protein spots that were significantly regulated by SQYZ treatment in 5XFAD mice. In the title line, Exp. Mr represented the experimental molecular weight of the proteins. Exp. pI represented the experimental isoelectric point of the proteins. The fold difference was represented by the ratio of the spot volume value of the Tg+SQYZ group to the value of the Tg+NS group.

0.05). These data revealed that SQYZ could reduce the specific pathological load in the AD brain.

SQYZ treatment exerted anti-inflammatory effect on the brains of AD transgenic mice

Glial activation, as a part of inflammatory responses, is an important phenotype of AD brains [19]. To determine the anti-inflammatory effect of SQYZ on 5XFAD mice, the expression level of the astrocyte marker GFAP and the microglial marker Iba1 were assessed by using immunofluorescent staining (**Figure 3A**). In the anti-GFAP and anti-Iba1 immunofluorescent staining, the fluorescence intensities in the cortices of the transgenic mice were much higher than in those of the WT mice ($P < 0.001$), indicating an inflammatory response in the brains of the AD transgenic mice. After the SQYZ or HupA treatment, the fluorescence intensities decreased significantly ($P < 0.05$) (**Figure 3B**, **3C**). In addition, there were no significant differences between the Tg+SQYZ and Tg+HupA groups. This finding suggested that the SQYZ treatment may inhibit inflammatory responses in the cortices of the AD transgenic mice.

Proteomic analysis revealed altered proteins level in SQYZ treated AD transgenic mouse model

To more comprehensively investigate the influence of SQYZ on AD process, 2-DE coupled with the MALDI-TOFMS/MS technique was applied to explore the differences between the proteomic profiles of the 5XFAD mice and the SQYZ-treated 5XFAD mice. Six replicated 2-DE

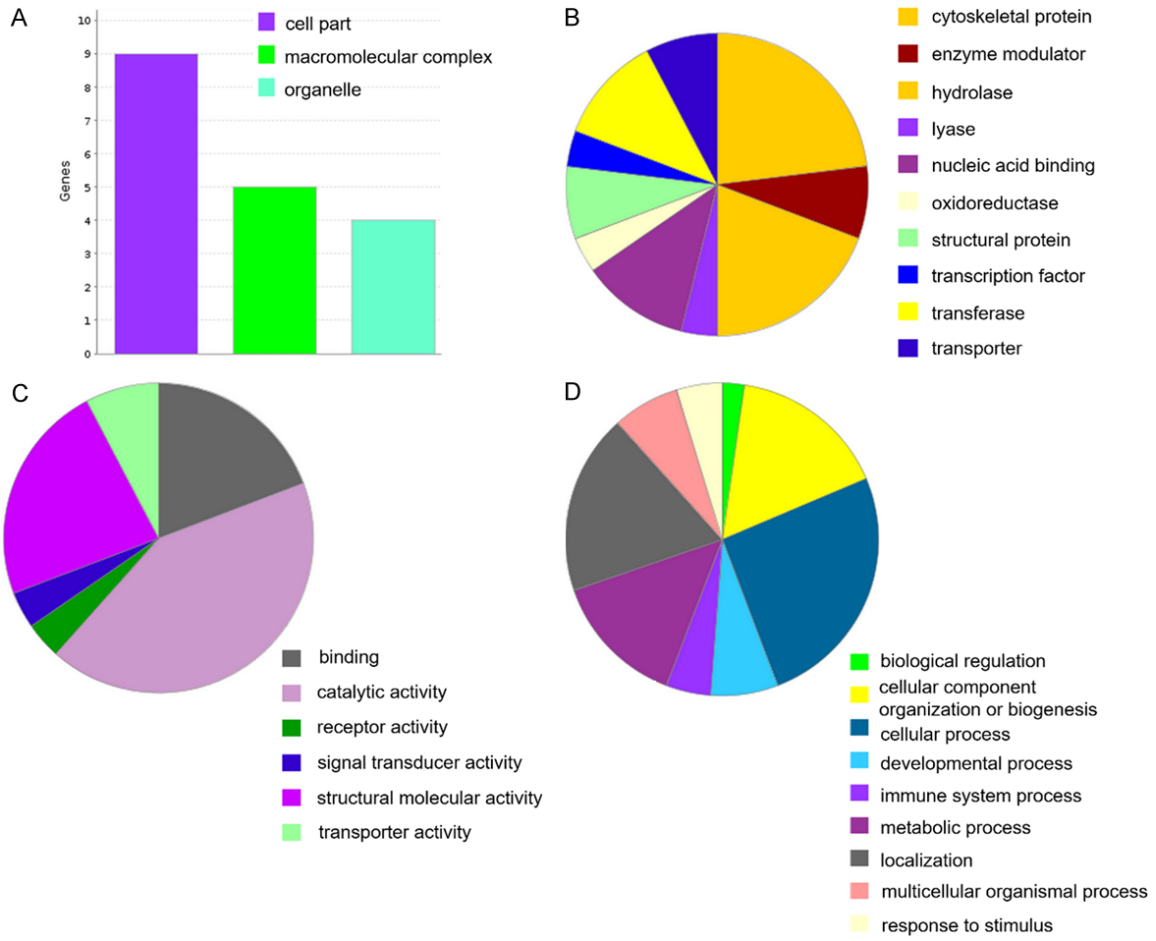

Figure 5. Gene ontology (GO) terms for cellular component, protein class, molecular function, and association of different essential biological process with differentially expressed proteins between Tg+NS and Tg+SQYZ group. Identified 27 proteins were classified according to (A) cellular component, (B) protein class, (C) molecular function, and (D) biological process in the PANTHER database.

gels collected from two independent groups (the Tg+NS group and the Tg+SQYZ group) were acquired. A total of 32 protein spots were successfully picked and identified using LC-MS/MS on each gel. Predominantly based on the comparison between the Tg+NS group and the Tg+SQYZ group, a total of 27 differentially expressed protein spots ($P < 0.05$ by Student's t-test) were selected and labelled with red arrows (**Figure 4A**, **4B**), with the criterion that the abundance change was at least 1.5-fold that of the changed protein spot volume. The detailed results were summarized in **Table 1**, including the target protein name, symbol, accession NO., exp. Mr, exp. pI, protein score, fold difference and *p* value. The fold changes were represented by the ratio of the spot volume of the Tg+SQYZ group to that of the Tg+NS group.

To confirm the results of the proteomic analysis, the expression levels of dynamin-1 and mitogen-activated protein kinase 3 (MAPK3) were measured by western blotting as representatives for all the differentially expressed proteins. Consistent with the proteomics results, MAPK3 was upregulated ($P < 0.05$) and dynamin-1 was down-regulated ($P < 0.01$) in the Tg+SQYZ mice compared to the Tg+NS mice (**Figure 4C**, **4D**).

Differentially expressed proteins could be functionally classified

To characterize the obtained proteins, a GO Slimmer analysis was performed to classify the proteins according to their cellular components, protein class, molecular function and biological process. Nearly half of them were intracellular proteins, and others localized to

Table 2. The functional category of differentially expressed proteins regulated by SQYZ in the cerebral cortex of 5XFAD mice

Protein name	Biological process	Subcellular location
Energy metabolism		
ATP synthase subunit beta, mitochondrial	Mitochondrial membrane ATP synthase produces ATP from ADP in the presence of a proton gradient across the membrane which is generated by electron transport complexes of the respiratory chain [46].	Mitochondrion, melanosome, nucleus, cell membrane
Dihydrolipoyllysine-residue acetyltransferase component of pyruvate dehydrogenase complex	The pyruvate dehydrogenase complex catalyzes the overall conversion of pyruvate to acetyl-CoA and CO_2, and thereby links the glycolytic pathway to the tricarboxylic cycle [47].	Mitochondrion matrix
Fatty acid binding protein 5, epidermal	High specificity for fatty acids, involved in glucose and lipid metabolic process [48].	Cytoplasm
Alpha-enolase	Multifunctional enzyme that, as well as its role in glycolysis, plays a part in various processes such as growth control, hypoxia tolerance and allergic responses [49].	Cytoplasm, cell membrane
Lactoylglutathione lyase	Catalyzes the conversion of hemimercaptal, formed from methylglyoxal and glutathione, to S-lactoylglutathione [50, 51].	Cytosol, extracellular exosome, nucleus, plasm membrane
L-lactate dehydrogenase B chain	Lactate biosynthetic process from pyruvate, involved in carbohydrate metabolic process [47].	Cytoplasm
DmX-like protein 1	Vacuolar acidification and proton-transporting V-type ATPase complex assembly [52].	RAVE complex
Stress response		
60 kDa heat shock protein, mitochondrial	Implicated in mitochondrial protein import and macromolecular assembly. May facilitate the correct folding of imported proteins [53, 54].	Mitochondrion matrix
Stress-70 protein, mitochondrial	Implicated in the control of cell proliferation and cellular aging [55]. May also act as a chaperone [56].	Mitochondrion
Heat shock cognate 71 kDa protein	Inhibits the transcriptional coactivator activity of CITED1 on Smad-mediated transcription. Chaperone [57].	Cytoplasm,
N(G), N(G)-dimethylarginine dimethylaminohydrolase	Hydrolyzes N(G), N(G)-dimethyl-L-arginine (ADMA) and N(G)-monomethyl-L-arginine (MMA) act as inhibitors of NOS [30].	Extracellular exosome, mitochondrion
Dephosphorylation		
Haloacid dehalogenase-like hydrolase domain-containing protein 2	Phosphatase activity	Extracellular exosome
DNA repair and transcription		
DNA repair and recombination protein RAD54-like	Involved in DNA repair and mitotic recombination. Functions in the recombinational DNA repair (RAD52) pathway [58].	Nucleus
Something about silencing protein 10	Essential for gene silencing-a role in the structure of silenced chromatin. Plays a role in the developing brain [59].	Nucleus
Transcriptional activator protein Pur-alpha	This is a probable transcription activator that specifically binds the purine-rich single strand of the PUR element located upstream of the c-Myc gene [60].	Nucleus
Axon guidance		
Dihydropyrimidinase-related protein 2	Plays a role in neuronal development and polarity, as well as in axon growth and guidance, neuronal growth cone collapse and cell migration [61].	Cytoplasm
Guanosine diphosphate (GDP) dissociation inhibitor 1	Regulates the GDP/GTP exchange reaction of most Rab proteins by inhibiting the dissociation of GDP from them, and the subsequent binding of GTP to them.	Cytoplasm, Golgi apparatus
Endocytosis		
Adaptin ear-binding coat-associated protein	NECAP endocytosis associated 1; Involved in endocytosis [62].	Cytoplasmic vesicle, cell membrane

Dynamin-1	Microtubule-associated force-producing protein involved in producing microtubule bundles and able to bind and hydrolyze GTP. Most probably involved in vesicular trafficking processes and receptor-mediated endocytosis [63].	Cytoplasm
Signal transduction		
Myozenin-2	Plays an important role in the modulation of calcineurin signaling. May play a role in myofibrillogenesis [64].	Cytoplasm
Olfactory marker protein	Acts as a modulator of the olfactory signal- transduction cascade [65]. Plays a role during olfactory neurogenesis [66].	Cytoplasm
Mitogen-activated protein kinase 3	Serine/threonine kinase, acting as an essential component of the MAP kinase signal transduction pathway [67].	Cytoplasm, nucleus, membrane
Cytoskeleton		
Tubulin beta-3 chain	Tubulin is the major constituent of microtubules.	Cytoplasm
Alpha-internexin	Internexin neuronal intermediate filament protein, alpha; Class-IV neuronal intermediate filament that is able to self-assemble. It is involved in the morphogenesis of neurons [68].	Cytoplasm, nucleus
Tropomodulin-2	Blocks the elongation and depolymerization of actin filaments. The Tmod/TM complex contributes to the formation of the short actin protofilament, which in turn defines the geometry of the membrane skeleton [69].	Cytoplasm
Tubulin beta-2A	Tubulin is the major constituent of microtubules. It binds two moles of GTP, one at an exchangeable site on the beta chain and one at a non-exchangeable site on the alpha chain.	Cytoplasm
Actin, cytoplasmic 1	Actins are highly conserved proteins that are involved in various types of cell motility.	Cytoplasm

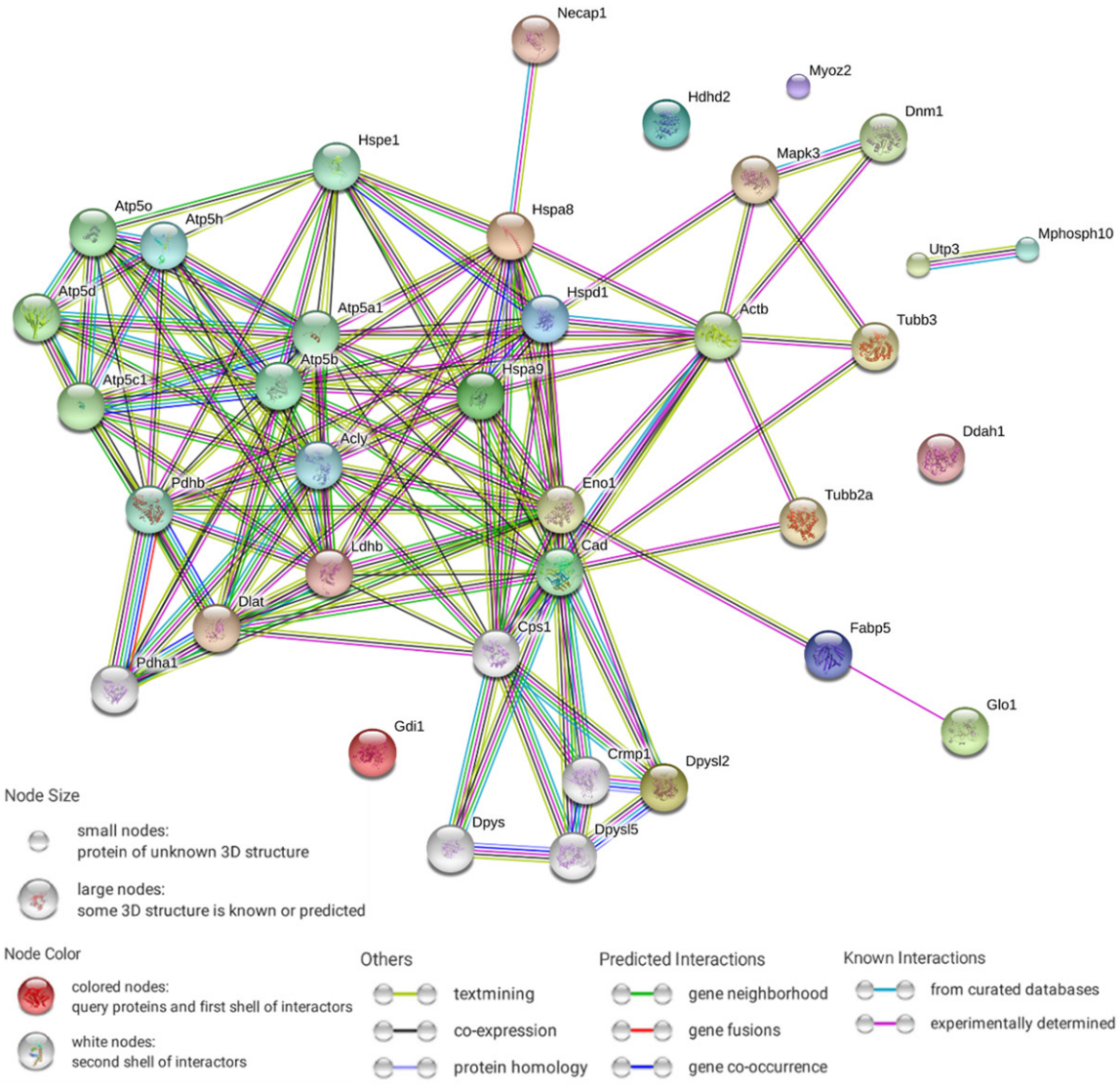

Figure 6. The constructed protein-protein interaction network of differentially expressed proteins identified between Tg+NS and Tg+SQYZ group. Twenty-two differentially expressed proteins identified were entered as focus to generate molecular networks using high-confidence mice interactions from the STRING database. Network nodes represent proteins: colored nodes, query proteins and first shell of interactors; white nodes, second shell of interactors; small nodes, proteins of unknown 3D structure; large nodes, some 3D structure is known or predicted. Edges represent protein-protein associations. The colors of edges refer to the type of evidence linking the corresponding proteins: cyanine, curated databases; purple, experimentally determined; green, gene neighborhood; red, gene fusion; dark blue, co-occurrence; black, co-expression; magenta, experiments; light green, text mining; mauve, homology.

macromolecular complexes or organelles (**Figure 5A**). Regarding the protein class classification, 23% of the obtained proteins were cytoskeletal protein, and 19% of them were hydrolases (**Figure 5B**). Among all the proteins, 40%, 22% and 19% of the proteins were found to have catalytic activity, structural molecule activity and binding activity, respectively (**Figure 5C**). Most of the proteins were determined to be involved in cellular or metabolic processes, and others were related to stimulus responses, immune system processes, localization, biological regulation and other biological processes (**Figure 5D**). Subsequently, these 27 proteins were classified to more specifically connect them to their biological functions (**Table 2**). Consistent with the GO Slim analysis, the list in **Table 2** showed that the SQYZ treatment influenced multiple biological functions, including energy metabolism, stress response, DNA

repair and transcription, endocytosis, dephosphorylation, axonal guidance, signal transduction and cytoskeleton. Among them, 7 proteins were related to energy metabolism, 5 proteins were related to the cytoskeleton, and 4 proteins were involved in immune responses and DNA repair and transcription. The protein expression level was increased in all cases after SQYZ treatment, except for the proteins related to endocytosis, one protein related to axonal guidance and one protein related to cytoskeleton. To explore the mechanical pathways involved in effects of SQYZ on the AD mouse model, the Ingenuity Pathway Analysis (IPA) was performed to construct a high-quality protein-protein interaction network containing 22 genes (**Figure 6**). The 22-protein interaction network identified here was rich in genes related to energy metabolism, immune response, and cytoskeleton. These analyses provided evidence that SQYZ might contribute to regulating energy production and stress responses at early stage of AD pathological process.

Discussion

The complexity of aetiology and pathogenesis of AD has been increasingly recognized in basic and clinical studies. More than 20 genetic loci associated with the risk of AD have been identified, and these are involved in immune system and inflammatory responses, cholesterol and lipid metabolism, and endosomal vesicle recycling [20]. Moreover, increasing evidence suggests that lifestyle-related factors have a role in AD, such as vascular health status, diabetes, obesity, physical and mental inactivity, depression, smoking, diet, and so on [5, 21]. Based on the complexity and multicausality of AD, the therapy of AD may be less promising by a single drug with a single target, and therefore aimed at multiple biological targets may be more hopeful. Traditional Chinese medicine (TCM) has a history of more than two thousand years in China. TCM preparations, composed of natural plants or natural plant extracts, have the advantages of being able to affect multiple targets and thus may be highly potent. TCM has been comprehensively applied in treatments of various diseases, such as diabetes, allergies, inflammation, and cancer. Many TCM herbal ingredients have been studied for their anti-AD effects, among which the excellent ones, such as galantamine and HupA, have even gained access to applications in clinics [22, 23]. These encouraging advancements indicate that TCM may be a promising candidate for the treatment of AD. SQYZ is raised under the theory of TCM and on the basis of a long history of clinical experience. It mainly consists of the ginsenoside Rg1, astragaloside A and baicalin, which have been well demonstrated to show potential efficacies against dementia [8, 9].

In this study, we investigated the therapeutic effects of SQYZ on an AD transgenic mouse model at the early phases of AD. As expected, SQYZ treatment markedly prevented behavioral impairments in the water maze, nest construction and passive avoidance tests. The results allow the conclusion to be drawn that SQYZ treatment effectively improves learning and memory abilities in AD mice. The alleviation of Aβ burden resulting from SQYZ treatment in the transgenic mouse brain implies that the SQYZ is an effective TCM preparations for the AD-like pathology. Because the pathogenesis of AD is complex, Aβ production and aggregation should not be the only intervention targets. In the current study, the 27 proteins successfully identified as differentially expressed by 2-DE and LC-MS/MS might include both direct SQYZ targets and downstream proteins. These 27 proteins could be classified into 8 groups based on their functions in energy metabolism, stress response, dephosphorylation, cytoskeleton, DNA repair and transcription, endocytosis, axon guidance and cell signaling.

Increasing evidence have suggested that the pathogenesis of AD is not restricted to the neuronal compartment but includes strong immunological mechanisms in the brain [24]. In AD process, neuroinflammation not only responds to pathophysiological events but also contributes to and drives AD pathogenesis [25, 26]. Microglia and astrocytes are key players in the inflammatory response of the brain, whose activation might occur early in AD, even before Aβ deposition [27]. Reactive glia and inflammatory mediators contribute to the disease progression. In the present work, SQYZ showed anti-inflammatory effects by suppressing the activation of microglia and astrocytes in the cortex. In addition, cytokines, one kind of neuroinflammatory mediator, stimulate inducible nitric oxide synthase (iNOS) in microglia and astrocytes, which produce high concentrations of nitric

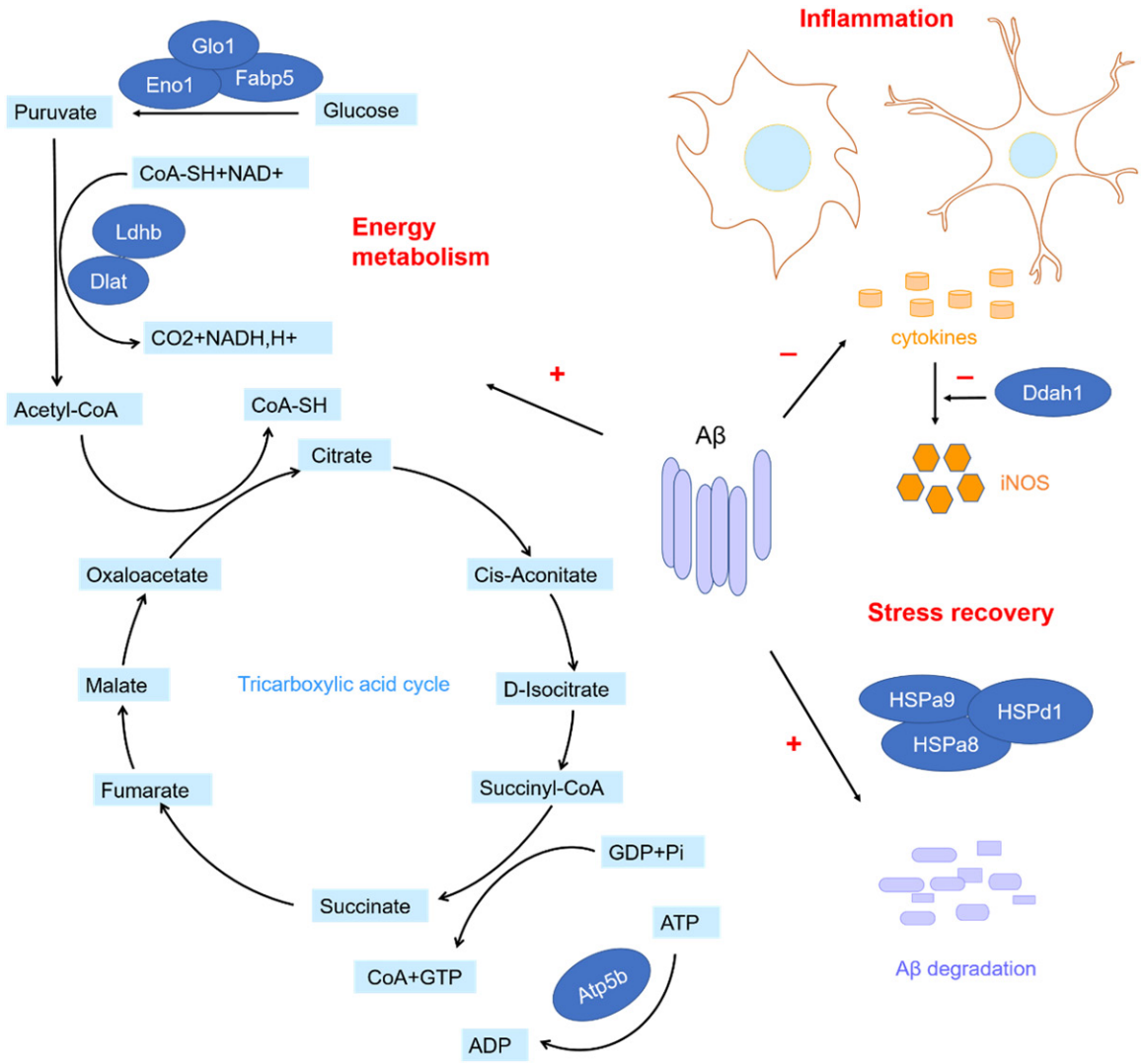

Figure 7. The likely mechanisms and potential targets of SQYZ in AD. The upregulated effects of SQYZ on energy metabolism and stress response related protein were represented by plus sign. The minus sign represented the inflammatory inhibition action of SQYZ in AD. The identified proteins were coloured in deep blue. Ddha1, dimethylarginine dimethylaminohydrolase; Glo1, lactoylglutathione lyase; Eno1, alpha-enolase; Fabp5, fatty acid binding protein 5; Ldhb, l-lactate dehydrogenase B chain; Dlat, dihydrolipoyllysine-residue acetyltransferase component of pyruvate dehydrogenase complex; Atp5b, ATP synthase subunit beta; HSPa9, stress-70 protein; HSPa8, heat shock cognate 71 kDa protein; HSPd1, 60 kDa heat shock protein.

oxide that are capable of neurotoxicity [28, 29]. Through proteomic analysis, we found that SQYZ treatment upregulated the level of dimethylarginine dimethylaminohydrolase (Ddah1), which acts as an inhibitor of NOS [30]. This result also suggests an anti-inflammatory role for SQYZ. In addition, the extract molecular mechanism remains to be further explored.

In addition to being phagocytosed by microglia and astrocytes, Aβ can also be removed from the brain by the chaperone-mediated autophagy (CMA) system [31]. Upon stress, heat shock proteins (HSPs), as molecular chaperones, bind to abnormal proteins and assist them to acquire native structure, thus preventing misfolding and the aggregation process [32, 33]. Sufficient evidence has suggested that HSPs act as critical regulators of neurodegenerative processes and are correlated with protein misfolding in the brains of AD patients [32]. Among them, numerous convincing reports have supported the hypothesis that HSP70 may play a neuroprotective role by inhibiting Aβ oligomerization

and enhancing the clearance of Aβ [34, 35]. Of our identified, differentially expressed proteins, heat shock cognate 71-kDa protein and stress-70 protein belong to the HSP70 class, and 60 kDa heat shock protein belongs to the HSP60 class. After SQYZ treatment, these three HSPs were all upregulated in the brain, indicating that the upregulation of HSPs might be a reason for the decreased Aβ burden in the brains of mice treated with SQYZ.

As far as energy metabolism is concerned, there is abundant literature that has reported that perturbed bioenergetic function, especially energy metabolic disturbances caused by mitochondrial dysfunction, has been observed in the brains and peripheral tissues of patients with mild cognitive impairment (MCI) and AD [36-38]. The disruption of energy metabolism is regarded as a prominent feature, a fundamental component and even a novel biomarker of AD [39-41]. Data have suspected that improving energy metabolism may be an effective way to prevent or treat brain ageing and AD [42-44]. In our study, the main differently expressed proteins associated with the energy metabolism include mitochondrial membrane ATP synthase (Atp5b), dihydrolipoyllysine-residue acetyltransferase component of pyruvate dehydrogenase complex (Dlat), fatty acid binding protein 5 (Fabp5), L-lactate dehydrogenase B chain (Ldhb), alpha-enolase (Eno1), lactoylglutathione lyase (Glo1) and DmX-like protein 1 (Dmxl1). It has been reported in a number of independent studies that these proteins participate in energy metabolic processes and play a central role in metabolic regulation. The levels of tricarboxylic acid (TCA) cycle metabolites were found to be significantly reduced in the CSF samples of AD patients compared to those of the MCI patients [45]. The enzymes and proteins involved in TCA cycle, including Dalt, Fabp5, Ldhb, Glo1 and Eno1, were upregulated by the SQYZ treatment in AD. Moreover, SQYZ treatment could improve mitochondrial energy metabolism by modulating the expressions of mitochondrial proteins, such as Atp5b and Dmxl1. In the present study, the increased expression levels of these proteins may have been conducive to improving energy metabolism.

The data in the present study suggest that SQYZ can improve the cognitive impairments and mitigate the pathological changes in the brain in AD transgenic mice, and this effect may be achieved through SQYZ's modulation of multiple processes related to AD pathogenesis, including Aβ deposition, neuroinflammation, stress responses, energy metabolism, etc. The suggested systemic model of SQYZ activity is summarized in **Figures 6** and **7**. However, it is still difficult to know which proteins are the direct targets of SQYZ and which are indirectly modulated. To clarify this, further studies may be necessary.

Acknowledgements

This work was supported by the State Key Program of National Natural Science of China (grant number: 81430100), National Science Fund for Distinguished Young Scholars (grant number: 81625025), Beijing New Medical Discipline Based Group (grant number: 100270569).

Disclosure of conflict of interest

None.

Address correspondence to: Xiaomin Wang, Department of Neurobiology, Capital Medical University, Key Laboratory for Neurodegenerative Disorders of The Chinese Ministry of Education, Beijing Institute for Brain Disorders, 10# Xitoutiao, Youanmenwai, Fengtai District, Beijing 100069, China. E-mail: xmwang@ccmu.edu.cn

References

[1] Shah H, Albanese E, Duggan C, Rudan I, Langa KM, Carrillo MC, Chan KY, Joanette Y, Prince M, Rossor M, Saxena S, Snyder HM, Sperling R, Varghese M, Wang H, Wortmann M and Dua T. Research priorities to reduce the global burden of dementia by 2025. Lancet Neurol 2016; 15: 1285-1294.

[2] Karran E, Mercken M and De Strooper B. The amyloid cascade hypothesis for Alzheimer's disease: an appraisal for the development of therapeutics. Nat Rev Drug Discov 2011; 10: 698-712.

[3] Boyle PA, Wilson RS, Yu L, Barr AM, Honer WG, Schneider JA and Bennett DA. Much of late life cognitive decline is not due to common neurodegenerative pathologies. Ann Neurol 2013; 74: 478-489.

[4] Frere S and Slutsky I. Alzheimer's disease: from firing instability to homeostasis network collapse. Neuron 2018; 97: 32-58.

[5] Scheltens P, Blennow K, Breteler MMB, de Strooper B, Frisoni GB, Salloway S and Van der

Flier WM. Alzheimer's disease. Lancet 2016; 388: 505-517.
[6] Sun X, Jin L and Ling P. Review of drugs for Alzheimer's disease. Drug Discov Ther 2012; 6: 285-290.
[7] Huang Y and Mucke L. Alzheimer mechanisms and therapeutic strategies. Cell 2012; 148: 1204-1222.
[8] Sreenivasmurthy SG, Liu JY, Song JX, Yang CB, Malampati S, Wang ZY, Huang YY and Li M. Neurogenic traditional Chinese medicine as a promising strategy for the treatment of Alzheimer's disease. Int J Mol Sci 2017; 18: 1-17.
[9] Gao J, Inagaki Y, Li X, Kokudo N and Tang W. Research progress on natural products from traditional Chinese medicine in treatment of Alzheimer's disease. Drug Discov Ther 2013; 7: 46-57.
[10] Wang Q, Xiao B, Cui SQ, Song HL, Qian YJ, Dong L, An HT, Cui YQ, Zhang WJ, He Y, Zhang JL, Yang J, Zhang FL, Hu GZ, Gong XL, Yan Z, Zheng Y and Wang XM. Triptolide treatment reduces Alzheimer's disease (AD)-like pathology through inhibition of BACE1 in a transgenic mouse model of AD. Dis Model Mech 2014; 7: 1385-1395.
[11] Sohanaki H, Baluchnejadmojarad T, Nikbakht F and Roghani M. Pelargonidin improves passive avoidance task performance in a rat amyloid beta25-35 model of Alzheimer's disease via estrogen receptor independent pathways. Acta Med Iran 2016; 54: 245-250.
[12] Deacon R. Assessing burrowing, nest construction, and hoarding in mice. J Vis Exp 2012; 59: e2607.
[13] Zheng Y, Wang Q, Xiao B, Lu Q, Wang Y and Wang X. Involvement of receptor tyrosine kinase Tyro3 in amyloidogenic APP processing and beta-amyloid deposition in Alzheimer's disease models. PLoS One 2012; 7: e39035.
[14] Wei DF, Tang JF, Bai WG, Wang YY and Zhang ZJ. Ameliorative effects of baicalein on an amyloid-beta induced Alzheimer's disease rat model: a proteomics study. Curr Alzheimer Res 2014; 11: 869-881.
[15] Candiano G, Bruschi M, Musante L, Santucci L, Ghiggeri GM, Carnemolla B, Orecchia P, Zardi L and Righetti PG. Blue silver: a very sensitive colloidal Coomassie G-250 staining for proteome analysis. Electrophoresis 2004; 25: 1327-1333.
[16] Rosengren AT, Salmi JM, Aittokallio T, Westerholm J, Lahesmaa R, Nyman TA and Nevalainen OS. Comparison of PDQuest and progenesis software packages in the analysis of two-dimensional electrophoresis gels. Proteomics 2003; 3: 1936-1946.
[17] Massignan T, Biasini E, Lauranzano E, Veglianese P, Pignataro M, Fioriti L, Harris DA, Salmona M, Chiesa R and Bonetto V. Mutant prion protein expression is associated with an alteration of the rab gdp dissociation inhibitor alpha (GDI)/Rab11 pathway. Mol Cell Proteomics 2010; 9: 611-622.
[18] Zhen J, Qian Y, Weng X, Su W, Zhang J, Cai L, Dong L, An H, Su R, Wang J, Zheng Y and Wang X. Gamma rhythm low field magnetic stimulation alleviates neuropathologic changes and rescues memory and cognitive impairments in a mouse model of Alzheimer's disease. Alzheimers Dement (N Y) 2017; 3: 487-497.
[19] Selkoe DJ. Alzheimer's disease: genes, proteins, and therapy. Physiol Rev 2001; 81: 741-766.
[20] Guerreiro R and Hardy J. Genetics of Alzheimer's disease. Neurotherapeutics 2014; 11: 732-737.
[21] Norton S, Matthews FE, Barnes DE, Yaffe K and Brayne C. Potential for primary prevention of Alzheimer's disease: an analysis of population-based data. Lancet Neurol 2014; 13: 1070-1070.
[22] Wang R, Yan H and Tang XC. Progress in studies of huperzine A, a natural cholinesterase inhibitor from Chinese herbal medicine. Acta Pharmacol Sin 2006; 27: 1-26.
[23] Takata K, Kitamura Y, Saeki M, Terada M, Kagitani S, Kitamura R, Fujikawa Y, Maelicke A, Tomimoto H, Taniguchi T and Shimohama S. Galantamine-induced amyloid-{beta} clearance mediated via stimulation of microglial nicotinic acetylcholine receptors. J Biol Chem 2010; 285: 40180-40191.
[24] Heneka MT, Carson MJ, Khoury JE, Landreth GE, Brosseron F, Feinstein DL, Jacobs AH, Wyss-Coray T, Vitorica J, Ransohoff RM, Herrup K, Frautschy SA, Finsen B, Brown GC, Verkhratsky A, Yamanaka K, Koistinaho J, Latz E, Halle A, Petzold GC, Town T, Morgan D, Shinohara ML, Perry VH, Holmes C, Bazan NG, Brooks DJ, Hunot S, Joseph B, Deigendesch N, Garaschuk O, Boddeke E, Dinarello CA, Breitner JC, Cole GM, Golenbock DT and Kummer MP. Neuroinflammation in Alzheimer's disease. Lancet Neurol 2015; 14: 388-405.
[25] Heppner FL, Ransohoff RM and Becher B. Immune attack: the role of inflammation in Alzheimer disease. Nat Rev Neurosci 2015; 16: 358-372.
[26] Sims R, van der Lee SJ, Naj AC, Bellenguez C, Badarinarayan N, Jakobsdottir J, Kunkle BW, Boland A, Raybould R, Bis JC, Martin ER, Grenier-Boley B, Heilmann-Heimbach S, Chouraki V, Kuzma AB, Sleegers K, Vronskaya M, Ruiz A, Graham RR, Olaso R, Hoffmann P, Grove ML, Vardarajan BN, Hiltunen M, Nothen MM, White CC, Hamilton-Nelson KL, Epelbaum J, Maier W, Choi SH, Beecham GW, Dulary C, Herms S, Smith AV, Funk CC, Derbois C,

Forstner AJ, Ahmad S, Li H, Bacq D, Harold D, Satizabal CL, Valladares O, Squassina A, Thomas R, Brody JA, Qu L, Sanchez-Juan P, Morgan T, Wolters FJ, Zhao Y, Garcia FS, Denning N, Fornage M, Malamon J, Naranjo MCD, Majounie E, Mosley TH, Dombroski B, Wallon D, Lupton MK, Dupuis J, Whitehead P, Fratiglioni L, Medway C, Jian X, Mukherjee S, Keller L, Brown K, Lin H, Cantwell LB, Panza F, McGuinness B, Moreno-Grau S, Burgess JD, Solfrizzi V, Proitsi P, Adams HH, Allen M, Seripa D, Pastor P, Cupples LA, Price ND, Hannequin D, Frank-Garcia A, Levy D, Chakrabarty P, Caffarra P, Giegling I, Beiser AS, Giedraitis V, Hampel H, Garcia ME, Wang X, Lannfelt L, Mecocci P, Eiriksdottir G, Crane PK, Pasquier F, Boccardi V, Henandez I, Barber RC, Scherer M, Tarraga L, Adams PM, Leber M, Chen Y, Albert MS, Riedel-Heller S, Emilsson V, Beekly D, Braae A, Schmidt R, Blacker D, Masullo C, Schmidt H, Doody RS, Spalletta G, Longstreth WT Jr, Fairchild TJ, Bossu P, Lopez OL, Frosch MP, Sacchinelli E, Ghetti B, Yang Q, Huebinger RM, Jessen F, Li S, Kamboh MI, Morris J, Sotolongo-Grau O, Katz MJ, Corcoran C, Dunstan M, Braddel A, Thomas C, Meggy A, Marshall R, Gerrish A, Chapman J, Aguilar M, Taylor S, Hill M, Fairen MD, Hodges A, Vellas B, Soininen H, Kloszewska I, Daniilidou M, Uphill J, Patel Y, Hughes JT, Lord J, Turton J, Hartmann AM, Cecchetti R, Fenoglio C, Serpente M, Arcaro M, Caltagirone C, Orfei MD, Ciaramella A, Pichler S, Mayhaus M, Gu W, Lleo A, Fortea J, Blesa R, Barber IS, Brookes K, Cupidi C, Maletta RG, Carrell D, Sorbi S, Moebus S, Urbano M, Pilotto A, Kornhuber J, Bosco P, Todd S, Craig D, Johnston J, Gill M, Lawlor B, Lynch A, Fox NC, Hardy J, Consortium A, Albin RL, Apostolova LG, Arnold SE, Asthana S, Atwood CS, Baldwin CT, Barnes LL, Barral S, Beach TG, Becker JT, Bigio EH, Bird TD, Boeve BF, Bowen JD, Boxer A, Burke JR, Burns JM, Buxbaum JD, Cairns NJ, Cao C, Carlson CS, Carlsson CM, Carney RM, Carrasquillo MM, Carroll SL, Diaz CC, Chui HC, Clark DG, Cribbs DH, Crocco EA, DeCarli C, Dick M, Duara R, Evans DA, Faber KM, Fallon KB, Fardo DW, Farlow MR, Ferris S, Foroud TM, Galasko DR, Gearing M, Geschwind DH, Gilbert JR, Graff-Radford NR, Green RC, Growdon JH, Hamilton RL, Harrell LE, Honig LS, Huentelman MJ, Hulette CM, Hyman BT, Jarvik GP, Abner E, Jin LW, Jun G, Karydas A, Kaye JA, Kim R, Kowall NW, Kramer JH, LaFerla FM, Lah JJ, Leverenz JB, Levey AI, Li G, Lieberman AP, Lunetta KL, Lyketsos CG, Marson DC, Martiniuk F, Mash DC, Masliah E, McCormick WC, McCurry SM, McDavid AN, McKee AC, Mesulam M, Miller BL, Miller CA, Miller JW, Morris JC, Murrell JR, Myers AJ, O'Bryant S, Olichney JM, Pankratz VS, Parisi JE, Paulson HL, Perry W, Peskind E, Pierce A, Poon WW, Potter H, Quinn JF, Raj A, Raskind M, Reisberg B, Reitz C, Ringman JM, Roberson ED, Rogaeva E, Rosen HJ, Rosenberg RN, Sager MA, Saykin AJ, Schneider JA, Schneider LS, Seeley WW, Smith AG, Sonnen JA, Spina S, Stern RA, Swerdlow RH, Tanzi RE, Thornton-Wells TA, Trojanowski JQ, Troncoso JC, Van Deerlin VM, Van Eldik LJ, Vinters HV, Vonsattel JP, Weintraub S, Welsh-Bohmer KA, Wilhelmsen KC, Williamson J, Wingo TS, Woltjer RL, Wright CB, Yu CE, Yu L, Garzia F, Golamaully F, Septier G, Engelborghs S, Vandenberghe R, De Deyn PP, Fernadez CM, Benito YA, Thonberg H, Forsell C, Lilius L, Kinhult-Stahlbom A, Kilander L, Brundin R, Concari L, Helisalmi S, Koivisto AM, Haapasalo A, Dermecourt V, Fievet N, Hanon O, Dufouil C, Brice A, Ritchie K, Dubois B, Himali JJ, Keene CD, Tschanz J, Fitzpatrick AL, Kukull WA, Norton M, Aspelund T, Larson EB, Munger R, Rotter JI, Lipton RB, Bullido MJ, Hofman A, Montine TJ, Coto E, Boerwinkle E, Petersen RC, Alvarez V, Rivadeneira F, Reiman EM, Gallo M, O'Donnell CJ, Reisch JS, Bruni AC, Royall DR, Dichgans M, Sano M, Galimberti D, St George-Hyslop P, Scarpini E, Tsuang DW, Mancuso M, Bonuccelli U, Winslow AR, Daniele A, Wu CK; Gerad/Perades CAE, Peters O, Nacmias B, Riemenschneider M, Heun R, Brayne C, Rubinsztein DC, Bras J, Guerreiro R, Al-Chalabi A, Shaw CE, Collinge J, Mann D, Tsolaki M, Clarimon J, Sussams R, Lovestone S, O'Donovan MC, Owen MJ, Behrens TW, Mead S, Goate AM, Uitterlinden AG, Holmes C, Cruchaga C, Ingelsson M, Bennett DA, Powell J, Golde TE, Graff C, De Jager PL, Morgan K, Ertekin-Taner N, Combarros O, Psaty BM, Passmore P, Younkin SG, Berr C, Gudnason V, Rujescu D, Dickson DW, Dartigues JF, DeStefano AL, Ortega-Cubero S, Hakonarson H, Campion D, Boada M, Kauwe JK, Farrer LA, Van Broeckhoven C, Ikram MA, Jones L, Haines JL, Tzourio C, Launer LJ, Escott-Price V, Mayeux R, Deleuze JF, Amin N, Holmans PA, Pericak-Vance MA, Amouyel P, van Duijn CM, Ramirez A, Wang LS, Lambert JC, Seshadri S, Williams J and Schellenberg GD. Rare coding variants in PLCG2, ABI3, and TREM2 implicate microglial-mediated innate immunity in Alzheimer's disease. Nat Genet 2017; 49: 1373-1384.

[27] Olabarria M, Noristani HN, Verkhratsky A and Rodriguez JJ. Concomitant astroglial atrophy and astrogliosis in a triple transgenic animal model of Alzheimer's disease. Glia 2010; 58: 831-838.

[28] Nathan C, Calingasan N, Nezezon J, Ding A, Lucia MS, La Perle K, Fuortes M, Lin M, Ehrt S,

Kwon NS, Chen J, Vodovotz Y, Kipiani K and Beal MF. Protection from Alzheimer's-like disease in the mouse by genetic ablation of inducible nitric oxide synthase. J Exp Med 2005; 202: 1163-1169.
[29] Vodovotz Y, Lucia MS, Flanders KC, Chesler L, Xie QW, Smith TW, Weidner J, Mumford R, Webber R, Nathan C, Roberts AB, Lippa CF and Sporn MB. Inducible nitric oxide synthase in tangle-bearing neurons of patients with Alzheimer's disease. J Exp Med 1996; 184: 1425-1433.
[30] Leiper J, Nandi M, Torondel B, Murray-Rust J, Malaki M, O'Hara B, Rossiter S, Anthony S, Madhani M, Selwood D, Smith C, Wojciak-Stothard B, Rudiger A, Stidwill R, McDonald NQ and Vallance P. Disruption of methylarginine metabolism impairs vascular homeostasis. Nat Med 2007; 13: 198-203.
[31] VanSlyke JK and Musil LS. Dislocation and degradation from the ER are regulated by cytosolic stress. J Cell Biol 2002; 157: 381-394.
[32] Lu RC, Tan MS, Wang H, Xie AM, Yu JT and Tan L. Heat shock protein 70 in Alzheimer's disease. Biomed Res Int 2014; 2014: 435203.
[33] Paul S and Mahanta S. Association of heat-shock proteins in various neurodegenerative disorders: is it a master key to open the therapeutic door? Mol Cell Biochem 2014; 386: 45-61.
[34] Hoshino T, Murao N, Namba T, Takehara M, Adachi H, Katsuno M, Sobue G, Matsushima T, Suzuki T and Mizushima T. Suppression of Alzheimer's disease-related phenotypes by expression of heat shock protein 70 in mice. J Neurosci 2011; 31: 5225-5234.
[35] Repalli J and Meruelo D. Screening strategies to identify HSP70 modulators to treat Alzheimer's disease. Drug Des Devel Ther 2015; 9: 321-331.
[36] Silva DF, Selfridge JE, Lu J, E L, Roy N, Hutfles L, Burns JM, Michaelis EK, Yan S, Cardoso SM and Swerdlow RH. Bioenergetic flux, mitochondrial mass and mitochondrial morphology dynamics in AD and MCI cybrid cell lines. Hum Mol Genet 2013; 22: 3931-3946.
[37] Swerdlow RH. Mitochondria and cell bioenergetics: increasingly recognized components and a possible etiologic cause of Alzheimer's disease. Antioxid Redox Signal 2012; 16: 1434-1455.
[38] Touchon J and Portet F. Mild cognitive impairment. Presse Med 2007; 36: 1464-1468.
[39] Mapstone M, Cheema AK, Fiandaca MS, Zhong XG, Mhyre TR, MacArthur LH, Hall WJ, Fisher SG, Peterson DR, Haley JM, Nazar MD, Rich SA, Berlau DJ, Peltz CB, Tan MT, Kawas CH and Federoff HJ. Plasma phospholipids identify antecedent memory impairment in older adults. Nat Med 2014; 20: 415-418.
[40] Sullivan PG and Brown MR. Mitochondrial aging and dysfunction in Alzheimer's disease. Prog Neuropsychopharmacol Biol Psychiatry 2005; 29: 407-410.
[41] Trushina E and Mielke MM. Recent advances in the application of metabolomics to Alzheimer's disease. Biochim Biophys Acta 2014; 1842: 1232-1239.
[42] Demetrius LA and Driver J. Alzheimer's as a metabolic disease. Biogerontology 2013; 14: 641-649.
[43] Kapogiannis D and Mattson MP. Disrupted energy metabolism and neuronal circuit dysfunction in cognitive impairment and Alzheimer's disease. Lancet Neurol 2011; 10: 187-198.
[44] Mamelak M. Sporadic Alzheimer's disease: the starving brain. J Alzheimers Dis 2012; 31: 459-474.
[45] Trushina E, Dutta T, Persson XMT, Mielke MM and Petersen RC. Identification of altered metabolic pathways in plasma and CSF in mild cognitive impairment and alzheimer's disease using metabolomics. PLoS One 2013; 8: e63644.
[46] Fliedner SM, Yang C, Thompson E, Abu-Asab M, Hsu CM, Lampert G, Eiden L, Tischler AS, Wesley R, Zhuang Z, Lehnert H and Pacak K. Potential therapeutic target for malignant paragangliomas: ATP synthase on the surface of paraganglioma cells. Am J Cancer Res 2015; 5: 1558-1570.
[47] Yasue M, Serikawa T and Yamada J. Chromosomal assignments of 23 biochemical loci of the rat by using rat x mouse somatic-cell hybrids. Cytogenet Cell Genet 1991; 57: 142-148.
[48] Maeda K, Uysal KT, Makowski L, Gorgun CZ, Atsumi G, Parker RA, Bruning J, Hertzel AV, Bernlohr DA and Hotamisligil GS. Role of the fatty acid binding protein mal1 in obesity and insulin resistance. Diabetes 2003; 52: 300-307.
[49] Nakamura N, Dai Q, Williams J, Goulding EH, Willis WD, Brown PR and Eddy EM. Disruption of a spermatogenic cell-specific mouse enolase 4 (eno4) gene causes sperm structural defects and male infertility. Biol Reprod 2013; 88: 90.
[50] Belanger M, Yang J, Petit JM, Laroche T, Magistretti PJ and Allaman I. Role of the glyoxalase system in astrocyte-mediated neuroprotection. J Neurosci 2011; 31: 18338-18352.
[51] Stallings RL and Siciliano MJ. Confirmational, provisional, and/or regional assignment of 15 enzyme loci onto Chinese hamster autosomes 1, 2, and 7. Somatic Cell Genet 1981; 7: 683-698.
[52] Kawamura N, Sun-Wada GH and Wada Y. Loss of G2 subunit of vacuolar-type proton transporting ATPase leads to G1 subunit upregulation in the brain. Sci Rep 2015; 5: 14027.

[53] Levy-Rimler G, Viitanen P, Weiss C, Sharkia R, Greenberg A, Niv A, Lustig A, Delarea Y and Azem A. The effect of nucleotides and mitochondrial chaperonin 10 on the structure and chaperone activity of mitochondrial chaperonin 60. Eur J Biochem 2001; 268: 3465-3472.
[54] Viitanen PV, Lorimer GH, Seetharam R, Gupta RS, Oppenheim J, Thomas JO and Cowan NJ. Mammalian mitochondrial chaperonin-60 functions as a single toroidal ring. J Biol Chem 1992; 267: 695-698.
[55] Chen TH, Kambal A, Krysiak K, Walshauser MA, Raju G, Tibbitts JF and Walter MJ. Knockdown of Hspa9, a del (5q31.2) gene, results in a decrease in hematopoietic progenitors in mice. Blood 2011; 117: 1530-1539.
[56] Wadhwa R, Kaul SC, Ikawa Y and Sugimoto Y. Identification of a novel member of mouse hsp70 family. Its association with cellular mortal phenotype. J Biol Chem 1993; 268: 6615-6621.
[57] Yamagishi N, Ishihara K, Saito Y and Hatayama T. Hsp105 but not Hsp70 family proteins suppress the aggregation of heat-denatured protein in the presence of ADP. FEBS Lett 2003; 555: 390-396.
[58] Wesoly J, Agarwal S, Sigurdsson S, Bussen W, Van Komen S, Qin J, van Steeg H, van Benthem J, Wassenaar E, Baarends WM, Ghazvini M, Tafel AA, Heath H, Galjart N, Essers J, Grootegoed JA, Arnheim N, Bezzubova O, Buerstedde JM, Sung P and Kanaar R. Differential contributions of mammalian Rad54 paralogs to recombination, DNA damage repair, and meiosis. Mol Cell Biol 2006; 26: 976-989.
[59] Sakuma T, Li QL, Jin Y, Choi LB, Kim EG, Ito K, Ito Y, Nomura S and Bae SC. Cloning and expression pattern of a novel PEBP2 beta-binding protein (charged amino acid rich leucine zipper-1[Crl-1]) in the mouse. Mech Dev 2001; 104: 151-154.
[60] Gupta M, Sueblinvong V, Raman J, Jeevanandam V and Gupta MP. Single-stranded DNA-binding proteins PURalpha and PURbeta bind to a purine-rich negative regulatory element of the alpha-myosin heavy chain gene and control transcriptional and translational regulation of the gene expression. Implications in the repression of alpha-myosin heavy chain during heart failure. J Biol Chem 2003; 278: 44935-44948.
[61] Wakatsuki S, Saitoh F and Araki T. ZNRF1 promotes Wallerian degeneration by degrading AKT to induce GSK3B-dependent CRMP2 phosphorylation. Nat Cell Biol 2011; 13: 1415-1423.
[62] Ritter B, Philie J, Girard M, Tung EC, Blondeau F and McPherson PS. Identification of a family of endocytic proteins that define a new alpha-adaptin ear-binding motif. EMBO Rep 2003; 4: 1089-1095.
[63] Boumil RM, Letts VA, Roberts MC, Lenz C, Mahaffey CL, Zhang ZW, Moser T and Frankel WN. A missense mutation in a highly conserved alternate exon of dynamin-1 causes epilepsy in fitful mice. PLoS Genet 2010; 6: e1001046.
[64] Frey N, Barrientos T, Shelton JM, Frank D, Rutten H, Gehring D, Kuhn C, Lutz M, Rothermel B, Bassel-Duby R, Richardson JA, Katus HA, Hill JA and Olson EN. Mice lacking calsarcin-1 are sensitized to calcineurin signaling and show accelerated cardiomyopathy in response to pathological biomechanical stress. Nat Med 2004; 10: 1336-1343.
[65] Youngentob SL and Margolis FL. OMP gene deletion causes an elevation in behavioral threshold sensitivity. Neuroreport 1999; 10: 15-19.
[66] Choi PS, Zakhary L, Choi WY, Caron S, Alvarez-Saavedra E, Miska EA, McManus M, Harfe B, Giraldez AJ, Horvitz HR, Schier AF and Dulac C. Members of the miRNA-200 family regulate olfactory neurogenesis. Neuron 2008; 57: 41-55.
[67] Murphy LO, Smith S, Chen RH, Fingar DC and Blenis J. Molecular interpretation of ERK signal duration by immediate early gene products. Nat Cell Biol 2002; 4: 556-564.
[68] Yuan A, Rao MV, Kumar A, Julien JP and Nixon RA. Neurofilament transport in vivo minimally requires hetero-oligomer formation. J Neurosci 2003; 23: 9452-9458.
[69] Cox PR, Fowler V, Xu B, Sweatt JD, Paylor R and Zoghbi HY. Mice lacking Tropomodulin-2 show enhanced long-term potentiation, hyperactivity, and deficits in learning and memory. Mol Cell Neurosci 2003; 23: 1-12.

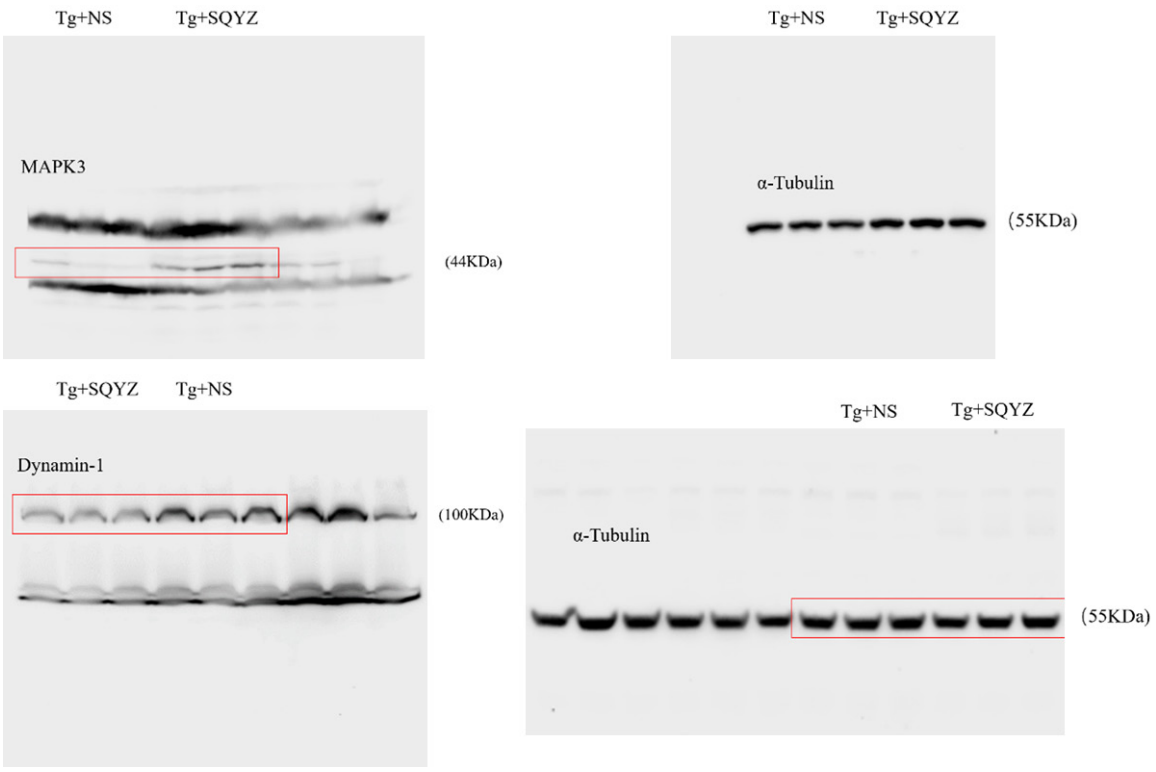

Supplementary Figure 1. Full immunoblots image of panels in **Figure 4**. Western examples were extracted from the cortices of the Tg+SQYZ and Tg+NS mice. Membranes were incubated with anti-MAPK antibody or anti-dynamin-1 antibody or antit-α-tubulin overnight. After incubation with secondary antibody, protein bands were visualized with the FluorChem E imaging system (protein simple).